IEEE Photonics Journal
An IEEE Photonics Society Publication

Highly Birefringent Two-Mode Photonic Crystal Fibers With Near-Zero Flattened Dispersion

Volume 3, Number 6, December 2011

Feifei Shi
Yun Wu
Meicheng Li
Yu Zhao
Liancheng Zhao

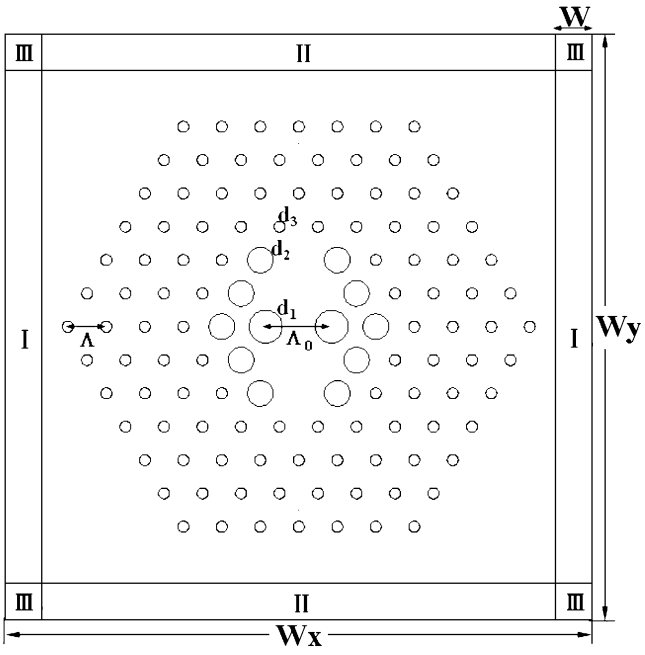

DOI: 10.1109/JPHOT.2011.2176480
1943-0655/$26.00 ©2011 IEEE

Highly Birefringent Two-Mode Photonic Crystal Fibers With Near-Zero Flattened Dispersion

Feifei Shi,[1] Yun Wu,[2] Meicheng Li,[1] Yu Zhao,[1] and Liancheng Zhao[1]

[1]Department of Information Materials Science and Technology, School of Materials Science and Engineering, Harbin Institute of Technology, Harbin 150001, China
[2]No. 52 Institute of China North Industry Group, Yantai 264003, China

DOI: 10.1109/JPHOT.2011.2176480

Manuscript received November 6, 2011; accepted November 9, 2011. Date of publication November 23, 2011; date of current version December 6, 2011. This work was supported in part by the program for New Century Excellent Talents in University (NCET) and project 2007 BAE15B04 supported by the National Science and Technology Ministry. Corresponding author: F. Shi (e-mail: gloria_ff@126.com).

Abstract: Through introducing three sizes of holes in cladding, highly birefringent two-mode photonic crystal fibers (PCFs) are proposed. The full-vector finite-element method (FEM) is applied in the calculation of the transverse electric field vector distributions of the two modes, their effective indices, modal birefringence, chromatic dispersion, and confinement losses. The defect holes near the core region are deliberately designed to obtain high birefringence. Furthermore, the structural parameters are carefully selected to flatten chromatic dispersion curve and reduce confinement losses.

Index Terms: Birefringence, chromatic dispersion, finite-element method (FEM), photonic crystal fibers (PCFs).

1. Introduction

The photonic crystal fiber (PCF), known as the "holey" fiber, is a microstructured fiber consisting of air hole arrays that run along the waveguide length of the fiber, which has unique properties that are not realized in standard optical fiber, such as endless single-mode operation [1], high birefringence [2], high nonlinearity and tailorable chromatic dispersion [3], and so on. The key point in realizing the birefringence is to destroy the symmetry of the fiber structure, which can be achieved either by altering the air hole sizes near the core area or by distorting the shape of the air holes (elliptical air holes) [4]–[6]. The stack-and-draw process is in favor of the former.

Birefringent two-mode optical fibers that support two stable spatial modes, i.e., the fundamental LP_{01} and the second-order even LP_{11} mode, have attracted considerable interest for a number of applications, including interferometric modal/polarimetric sensors of strain, temperature, or both at the same time [7], [8]. A kind of highly birefringent PCFs for two-mode devices is reported in the literature [9]. The birefringence in this structure is induced by two air holes adjacent to the fiber core and having diameter greater than the other cladding holes.

In this work, we employed the index-guiding PCF structure with uniform air-silica lattice, as well as the defected-core to achieve high birefringence and two-mode propagation. Based on the suitable sample, we optimized the design parameters to achieve other desirable properties, including high birefringence and near-zero flattened dispersion. The optimized structure was numerically analyzed by using full-vector finite-element method (FEM). The boundary conditions

were treated with anisotropic perfectly matched layers (PMLs) to minimize the reflections at the boundary and thus simulated an unbounded region.

2. Theory

2.1. Simulation Method

A full vectorial FEM formulation for modal analysis based on anisotropic PMLs is capable of handling as many other modes as required and analyzing the leaky modes. Using PMLs boundary conditions, propagation characteristics of leaky modes in PCF, as well as even both dispersion and loss properties, can be accurately evaluated [10], [11].

Using FEM, the PCF cross section, with the finite number of air holes, was divided into homogeneous subspaces where Maxwell's equations were solved by accounting for the adjacent subspaces. These subspaces are triangles that allow a good approximation of the circular structures. Using the anisotropic PML, from Maxwell's curl equations, the following vectorial equation was obtained:

$$\nabla \times \left([s]^{-1}\nabla \times \vec{E}\right) - k_0^2 n^2\,[s] \qquad \vec{E} = 0 \tag{1}$$

where $\vec{E}$ denotes the electric field. $k_0 = 2\pi/\lambda$ is the free space wave-number. n is the refractive index of the domain, [s] is the PML matrix, $[s]^{-1}$ is an inverse matrix of [s], and λ is the operating wavelength [10].

2.2. Birefringence

The birefringence of a PCF is determined by the difference between the real part of the effective indices $\mathrm{Re}(n_{eff}^x)$ and $\mathrm{Re}(n_{eff}^y)$, which corresponds to the two fundamental core eigenmodes LP_{01}^x and LP_{01}^y mainly polarized along the x- and y-axes, respectively

$$B = \left|\mathrm{Re}\left(n_{eff}^x\right) - \mathrm{Re}\left(n_{eff}^x\right)\right|. \tag{2}$$

2.3. Chromatic Dispersion

The Chromatic dispersion consists of material dispersion and waveguide dispersion, which can be calculated from the n_{eff} value against the wavelength using

$$D = -\left(\frac{\lambda}{c}\right)\frac{\partial^2 n_M}{\partial \lambda^2} - \left(\frac{\lambda}{c}\right)\frac{\partial^2\left[\mathrm{Re}(n_{eff})\big|_{n_M(\lambda)=const.}\right]}{\partial \lambda^2} \tag{3}$$

where c is the speed of light, and n_M is dependent on λ in dispersive media. The material dispersion is given by Sellmeier's formula [12].

When $n_M(\lambda) = const.$, material dispersion can be neglected. It is possible to alter the balance between the two dispersion mechanisms, and the desired dispersion profile can achieved by changing the structure parameters.

2.4. Confinement Loss

When the optical mode is propagating in the core region, due to a finite number of layers of air holes, the mode leakage from the core region into the outer air hole region is unavoidable, and then, the confinement loss due to the extent of the cladding is occurring. The confinement loss of the fundamental mode is calculated from the imaginary part of the complex effective index n_{eff}, using

$$\text{Conf. loss} = \frac{40\pi}{\ln(10)\lambda}\mathrm{Im}(n_{eff})\ [\text{dB/m}] \tag{4}$$

where Im is the imaginary part of the n_{eff} [13].

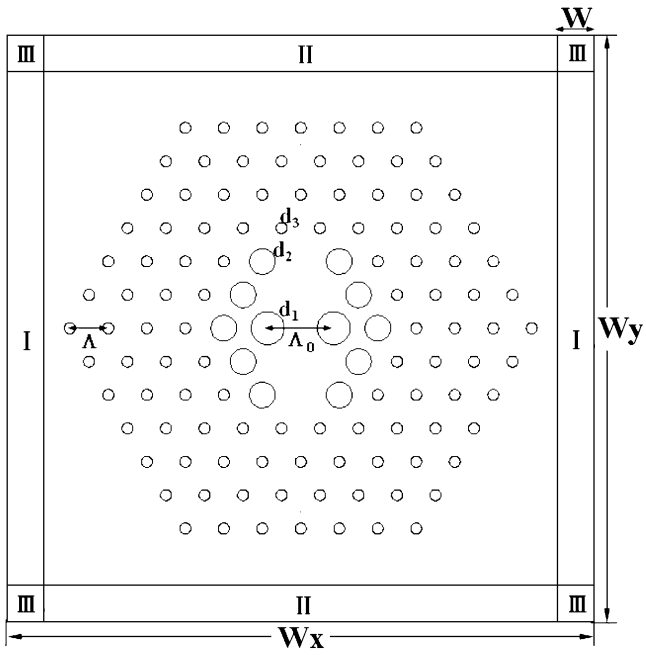

Fig. 1. Cross section of two-mode PCF.

3. Results and Discussions

3.1. Structure Parameters

It is well known that hexagonal structure is the best arrangement of air-holes to gain high birefringence, flatten dispersion, and get very low confinement loss. In this paper, we propose PCFs, which are shown in Fig. 1. The PCF comprises of a hexagonal lattice of air holes with missing holes on the inner rings in a silica background, whose refractive index is 1.45. There are four holes omitting on the first ring and two on the second. The outer four rings are in hexagonal symmetry. The diameter of air holes and hole-to-hole spacing is denoted with d and Λ. As shown in Fig. 1, $\Lambda_0 = 3.6$ μm is the distance of the biggest two holes in the center; $\Lambda = 2$ μm is the distance between each of the rings; and $d_1 = 1.8$ μm, $d_2 = 1.4$ μm, and $d_3 = d_4 = d_5 = d_6 = 0.6$ μm show the diameter of air holes on different rings, respectively. The computational window in x- and y-direction is $Wx = Wy = 26$ μm. The PML region, of which the thickness is 2 μm, is uniformly divided into eight subdivisions. These parameters are carefully selected to optimize the optical properties.

3.2. Modal Characteristics of the Two Modes

The calculated results indicate that, over a very wide wavelength range, as shown in Fig. 2, the PCF supports only four nondegenerate eigenmodes (LP^x_{01}, LP^y_{01}, LP^x_{11}, and LP^y_{11}) with transverse mode field pattern shown in Fig. 3. Besides two orthogonal polarization modes LP^x_{01} and LP^y_{01}, the second-order mode LP^x_{11} (even) and LP^y_{11} (even) can propagate stably in high birefringence PCF within the wavelength range of 0.4 μm to 2 μm, which covers almost the entire low loss window of the silica fibers. The mode effective index become low with the wavelength increasing. The index of the y-polarized is larger than that of the x-polarized one, and their gap is increasing with wavelength. As shown in Fig. 4, the birefringence reaches an order of 10^{-3}.

3.3. Influence of the Geometric Parameter Λ on Birefringence, Dispersion, and Confinement Losses

In this section, we investigate the influence of the geometric parameters Λ and d_2 on mode LP_{01}'s birefringence, dispersion, and confinement losses. However, the pitch Λ_0, d_1, and d_3 were kept

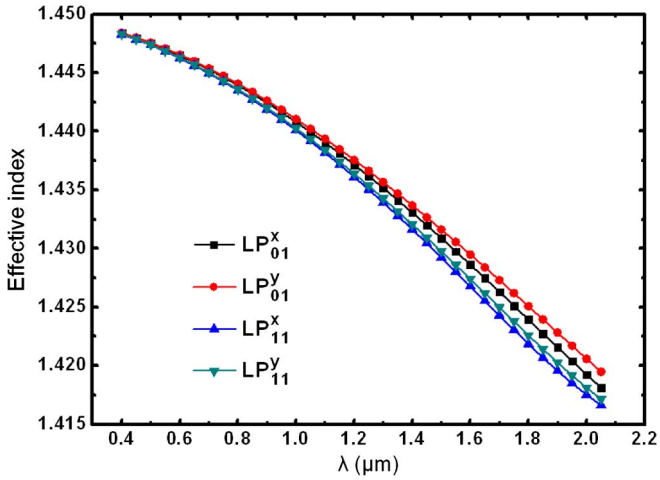

Fig. 2. Mode effective indexes of the fundamental and the second order modes as functions of wavelength.

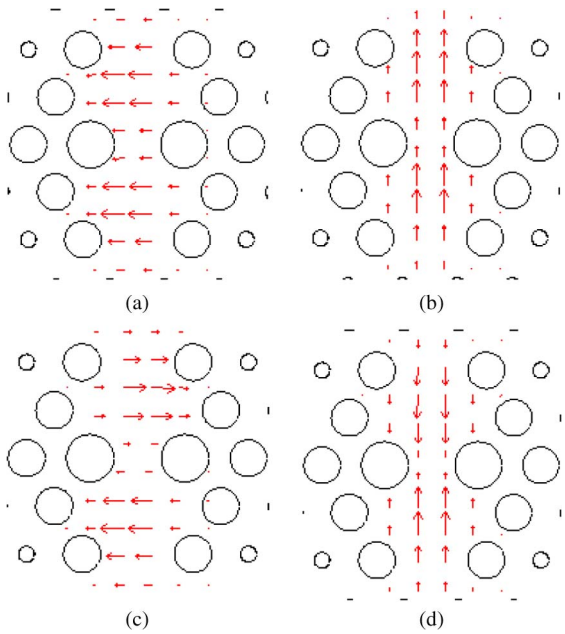

Fig. 3. Vector distribution of two guiding mode (a) and (b) LP_{01} and (c) and (d) LP_{11} (even). (a) LP^x_{01}. (b) LP^y_{01}. (c) LP^x_{11} (even). (d) LP^y_{11} (even).

constant for the whole study, which is necessary to keep a large enough d_1 and a close pitch Λ_0 for obtaining a high birefringence, as reported in much of the literature.

Fig. 4 shows the birefringence value by varying Λ from 1.8 μm to 2.2 μm when other parameters remain unchanged. The birefringence decreases with the increase of Λ. When Λ decreases to 1.9 μm, the birefringence reaches an order of 10^{-3} at 1.55 μm wavelength.

On the basis of the above analysis, we focus on optimizing flattened dispersion of LP^x_{01} mode. Fig. 5 shows the variation of the chromatic dispersion of LP^x_{01} mode as a function of the wavelength. The impact of tuning the pitch Λ on the total dispersion is illustrated with up-shifted dispersion curves at smaller pitch values. When $\Lambda = 2.05$ μm, near-zero flattened dispersion in a wide wavelength is obtained. Especially, the LP^x_{01} mode exhibits a dispersion of 0.196 ps/(km • nm) for 1.55 μm wavelength.

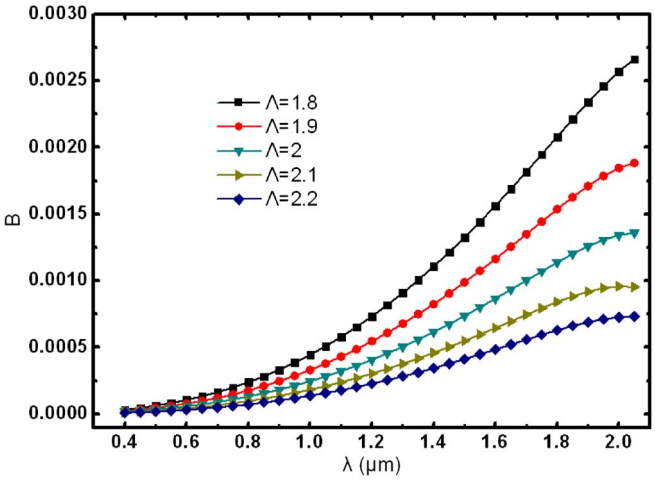

Fig. 4. Birefringence of the fundamental mode as functions of wavelength.

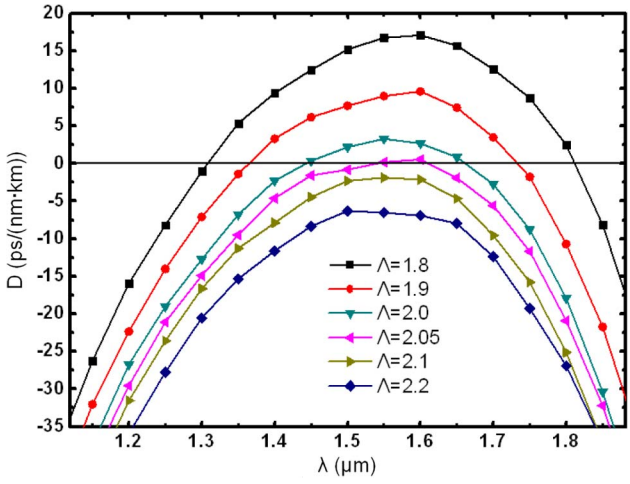

Fig. 5. Dispersion of the LP_{01}^{x} mode as functions of wavelength.

The confinement loss strongly depends on the number of air hole rings, air hole diameter, and hole-to-hole spacing. The confinement losses of the fundamental mode LP_{01}^{x} are presented in Fig. 6. According to the numerical simulation results, as the pitch Λ decreases, confinement losses of LP_{01}^{x} mode is reduced significantly. In the proposed design in Fig. 1, the confinement loss is 4.6E-5 dB/m at the operating wavelength $\lambda = 1.55$ μm.

Based on the simulation results, it is possible to obtain PCF with high birefringence and low confinement losses if Λ is further reduced, but this would have a unfavorable effect on the chromatic dispersion properties. Therefore, the tradeoff between near-zero flatten dispersion and other two properties should be take into account.

3.4. Influence of the Geometric Parameter d_2 on Birefringence, Dispersion, and Confinement Losses

As reported in much of the literature, increasing the outer air hole size or the number of rings, the mode becomes more confined, and confinement loss is reduced. At the same time, the influence of outer air holes on birefringence is not remarkable. We paid attention to the special inner ring air hole size d_2, while other parameters were kept constant, as in Fig. 1.

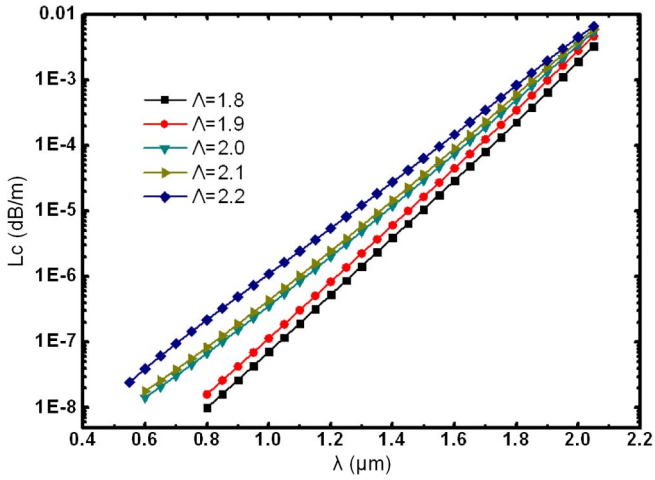

Fig. 6. Confinement losses of the LP_{01}^{x} mode as functions of wavelength.

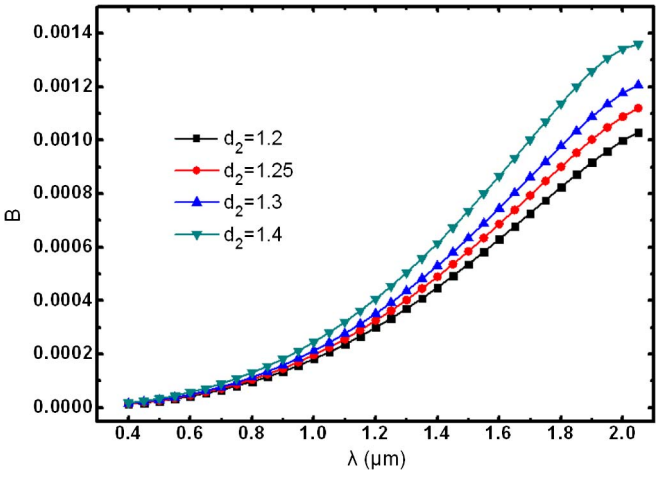

Fig. 7. Birefringence of the fundamental mode as functions of wavelength.

Increasing the second ring air hole diameter d_2 enhances B, as shown in Fig. 7, but the change is not obvious, compared with Fig. 4. As for confinement losses, the curves in Fig. 8 are almost coincident at shorter wavelengths, and the gaps are too slim for longer wavelengths, which is different from Fig. 6. A bigger d_2 helps to heighten the birefringence, but it is not helpful to lessen confinement losses. Moreover, the effect of d_2 are not as notable as that of Λ.

Choosing a proper parameter d_2, the chromatic dispersion of LP_{01}^{x} mode presents near-zero flattened, as shown in Fig. 9. When $d_2 = 1.25$ μm, the LP_{01}^{x} mode exhibits a dispersion of 0.196 ps/(km • nm) for 1.55 μm wavelength, and ultraflattened dispersion of $-0.8 \sim +0.2$ ps/(km • nm) is obtained in 1.5 to 1.65 μm wavelength range.

In the second air-hole ring, we omitted two holes and kept the diameter large enough to reduce the rotational symmetry of the fiber structure to obtain high birefringence. Furthermore, the simulation results indicate that parameter d_2 impacts the properties indistinctly, which will be helpful to simplify the requirement to fabrication technology.

3.5. Influence of Some Uncertainty in Fabrication on Birefringence

The preferred fabrication technique stack-and-draw was introduced by Birks in 1996 [14]. It allows relatively fast, clean, low-cost, and flexible preform manufacture, as reported in Fig. 10 [15].

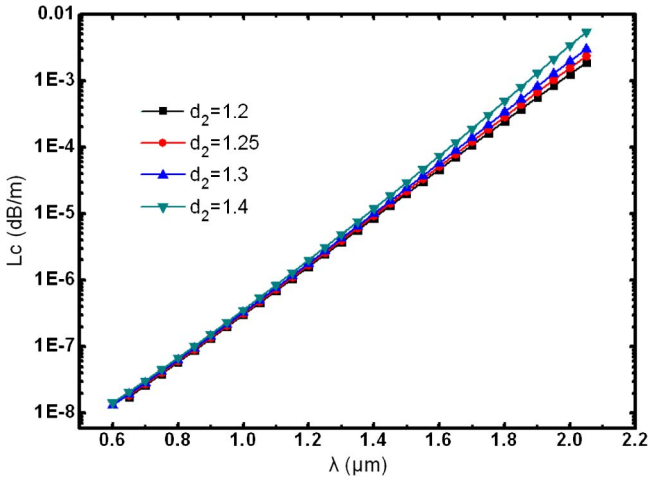

Fig. 8. Confinement losses of the LP_{01}^{x} mode as functions of wavelength.

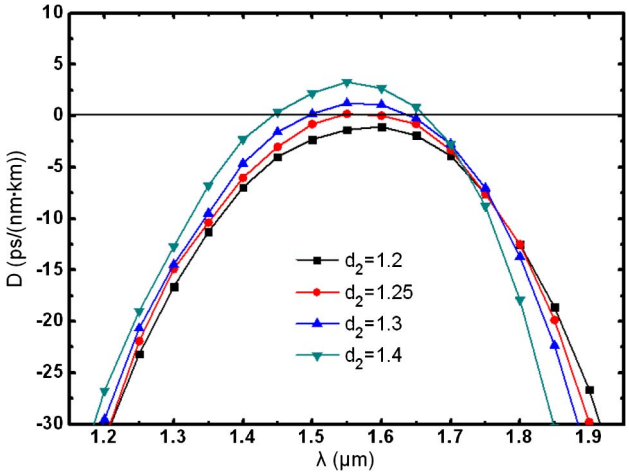

Fig. 9. Dispersion of the LP_{01}^{x} mode as functions of wavelength.

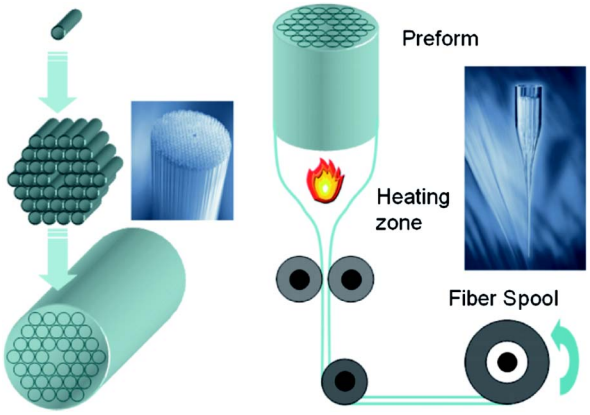

Fig. 10. Scheme of the PCF fabrication process [15].

Although the surface tension can otherwise lead the air-hole collapse, a slight overpressure relative to the surroundings may prevent it.

As reported in much of the literature [5], [6], the outer rings have almost no impact on the birefringence. So, we considered some uncertain variances of d_1 and d_2; moreover, the location and shape of holes on the inner two rings were taken into account. The results show that Λ and d_2 are the most sensitive parameters. A closer holes arrangement and bigger holes in the second ring bring us a considerable birefringence. As for the change in the symmetry, the diversification only in the polarization directions is permissible, whereas the alteration in the nonpolarization directions should be avoided. Furthermore, the small deformation of the holes induced by the production process have only a slight effect on the birefringence.

4. Conclusion

In this article, the novel PCFs have been analyzed based on the FEM. To induce high birefringence up to 1E-3 order, omitting inner two ring holes was used to destroy the symmetry of the structure. The proper air hole size and pitch help flat dispersion near zero. Ultraflattened dispersion of $-0.8 \sim 0.2$ ps$/$(km $\bullet$ nm) was obtained to within a 1.5 to 1.65 μm wavelength range. Especially, the structure supports two-modes over extremely broad wavelength ranges.

References

[1] T. A. Birks, J. C. Knight, and P. S. Russell, "Endlessly single-mode photonic crystal fiber," *Opt. Lett.*, vol. 22, no. 13, pp. 961–963, Jul. 1997.

[2] K. Saitoh and M. Koshiba, "Photonic bandgap fibers with high birefringence," *IEEE Photon. Technol. Lett.*, vol. 14, no. 9, pp. 1291–1293, Sep. 2002.

[3] T. Fujisawa and M. Koshiba, "Finite element characterization of chromatic dispersion in nonlinear holey fibers," *Opt. Express*, vol. 11, no. 13, pp. 1481–1489, Jun. 2003.

[4] M. J. Steel and R. M. Osgood, Jr., "Polarization and dispersive properties of elliptical-hole photonic crystal fibers," *J. Lightw. Technol.*, vol. 19, no. 4, pp. 495–503, Apr. 2001.

[5] T. P. Hansen, J. Broeng, S. E. B. Libori, E. Knudsen, A. Bjarklev, J. R. Jensen, and H. Simonsen, "Highly birefringent index-guiding photonic crystal fibers," *IEEE Photon. Technol. Lett.*, vol. 13, no. 6, pp. 588–590, Jun. 2001.

[6] A. Ortigosa-Blanch, J. C. Knight, W. J. Wadsworth, J. Arriaga, B. J. Mangan, T. A. Birks, and P. S. J. Russell, "Highly birefringent photonic crystal fibers," *Opt. Lett.*, vol. 25, no. 18, pp. 1325–1327, Sep. 2000.

[7] B. Y. Kim, J. N. Blake, S. Y. Huang, and H. J. Shaw, "Use of highly elliptical core fibers for two-mode fiber devices," *Opt. Lett.*, vol. 12, no. 9, pp. 729–731, Sep. 1987.

[8] J. N. Blake, S. Y. Huang, B. Y. Kim, and H. J. Shaw, "Strain effects on highly elliptical core two-mode fibers," *Opt. Lett.*, vol. 12, no. 9, pp. 732–734, Sep. 1987.

[9] W. Jin, Z. Wang, and J. Ju, "Two-mode photonic crystal fibers," *Opt. Express*, vol. 13, no. 6, pp. 2082–2088, Mar. 2005.

[10] K. Saitoh and M. Koshiba, "Full-vectorial imaginary-distance beam propagation method based on a finite element scheme: Application to photonic crystal fibres," *IEEE J. Quantum Electron.*, vol. 38, no. 7, pp. 927–933, Jul. 2002.

[11] S. Haxha and H. Ademgil, "Novel design of photonic crystal fibres with low confinement losses, nearly zero ultra-flatted chromatic dispersion, negative chromatic dispersion and improved effective mode area," *Opt. Commun.*, vol. 281, no. 2, pp. 278–286, Jan. 2008.

[12] A. Bjarklev, J. Broeng, and A. S. Bjarklev, *Photonic Crystal Fibers*. Dordrecht, The Netherlands: Kluwer, 2003.

[13] K. Saitoh and M. Koshiba, "Chromatic dispersion control in photonic crystal fibers: Application to ultra-flattened dispersion," *Opt. Express*, vol. 11, no. 8, pp. 843–852, Apr. 2003.

[14] T. A. Birks, D. M. Atkin, G. Wylangowski, P. S. J. Russell, and P. J. Roberts, "2D photonic band gap structures in fibre form," in *Photonic Band Gap Materials*, C. M. Soukoulis, Ed. Dordrecht, The Netherlands: Kluwer, 1996, pp. 437–444.

[15] F. Poli, A. Gucinotta, and S. Selleri, *Photonic Crystal Fibers: Properties and Applications*. New York: Springer-Verlag, 2007.